

On the Challenge of Exploring the Evolutionary Trajectory from Phosphotriesterase to Arylesterase Using Computer Simulations

Ram Prasad Bora,^{†,||} Matthew J. L. Mills,^{‡,||} Maria P. Frushicheva,^{§,||} and Arieh Warshel^{*,†}

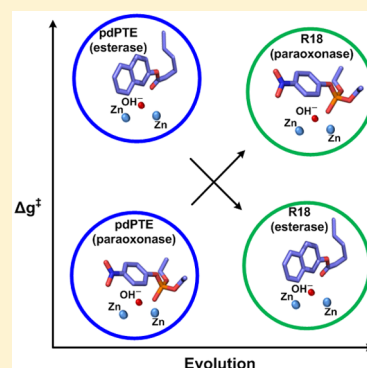
[†]Department of Chemistry, University of Southern California, 3620 McClintock Avenue, Los Angeles, California 90089, United States

[‡]Deconstruction Division, Joint BioEnergy Institute, Emeryville, California, United States & Biomass Science and Conversion Technology Department, Sandia National Laboratories, Livermore, California 94550, United States

[§]Department of Chemical Engineering, Massachusetts Institute of Technology, 25 Ames Street, Cambridge, Massachusetts 02142, United States

S Supporting Information

ABSTRACT: The ability to design effective enzymes presents a fundamental challenge in biotechnology and also in biochemistry. Unfortunately, most of the progress on this field has been accomplished by bringing the reactants to a reasonable orientation relative to each other, rather than by rational optimization of the polar preorganization of the environment, which is the most important catalytic factor. True computer based enzyme design would require the ability to evaluate the catalytic power of designed active sites. This work considers the evolution from a phosphotriesterase (with the paraoxon substrate) to arylesterase (with the 2-naphthylhexanoate (2NH) substrate) catalysis. Both the original and the evolved enzymes involve two zinc ions and their ligands, making it hard to obtain a reliable quantum mechanical description and then to obtain an effective free energy sampling. Furthermore, the options for the reaction path are quite complicated. To progress in this direction we started with DFT calculations of the energetics of different mechanistic options of cluster models and then used the results to calibrate empirical valence bond (EVB) models and to generate properly sampled free energy surfaces for different mechanisms in the enzyme. Interestingly, it is found that the catalytic effect depends on the Zn–Zn distance making the mechanistic analysis somewhat complicated. Comparing the activation barriers of paraoxon and the 2NH ester at the beginning and end of the evolutionary path reproduced the observed evolutionary trend. However, although our findings provide an advance in exploring the nature of promiscuous enzymes, they also indicate that modeling the reaction mechanism in the case of enzymes with a binuclear zinc center is far from trivial and presents a challenge for computer-aided enzyme design.



I. INTRODUCTION

Progress in the design of artificial enzymes is expected to play an important role in medical and industrial fields.^{1–4} Unfortunately, most attempts of enzyme design have not been led to highly effective enzymes.^{1,3} Furthermore, even the advances in directed evolution (e.g., refs 5–10) have not provided a clear understanding of the specific origins of rate enhancements resulting from these experiments. Thus, in our opinion the best way to identify the problems with current rational design strategies (e.g., see refs 1, 11–17) is to examine the performance of computer modeling of enzyme catalysis. Apparently, most of the existing studies have not been able to reproduce the relevant activation barriers and the corresponding rate constants. As we argued repeatedly,^{16,18–21} it seems to us that the problems with most current design attempts reflect incomplete and improper modeling of the relevant transition state (TS) and unfamiliarity with the key role of the polar reorganization in establishing the effect of mutations on catalysis.^{17,22}

Quantitative simulation strategy has been offered by the empirical valence bond (EVB) method (e.g., refs 19, 23). In

fact, computational studies of the effect of mutations on enzyme catalysis date back to EVB simulations of mutational effect in trypsin²⁴ and subsequent EVB studies of mutational effects (e.g., refs 19, 23, 25–27), as well as more recent molecular orbital-combined quantum mechanical/molecular mechanics (MO-QM/MM) works (e.g., refs 28–32). Some of the above works have established the importance of changes in reorganization energy upon mutation.^{19,22,26} Our work (ref 33) has examined the performance of the EVB in quantitative screening of design proposals. More recently, we demonstrated that the EVB can reproduce the results of directed evolution refinement of Kemp eliminases.^{20,21}

As pointed out in our previous studies,^{21,34} reactions such as the Kemp elimination are hard to catalyze since the change in charge distribution between the ground state and TS is relatively small. With this in mind, it is useful to consider reactions with larger changes in the charge distribution, as is

Received: December 12, 2014

Revised: January 15, 2015

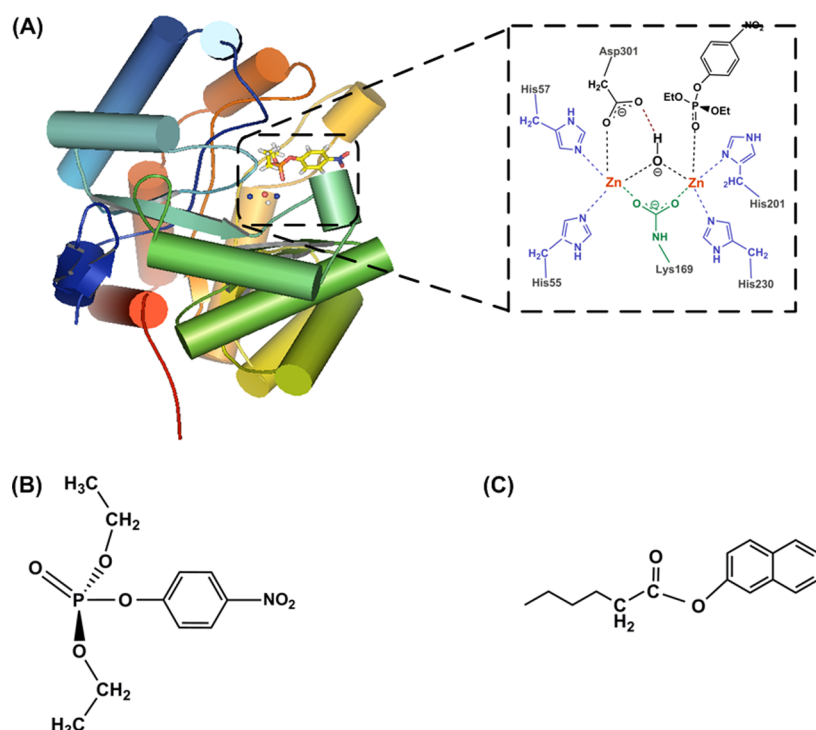


Figure 1. (A) Showing the structure of PTE with a docked substrate. The inset depicts schematically the substrate (paraoxon) and its active site environment. (B) and (C) depicts the chemical structures of paraoxon and 2-naphthyl hexanoate (2NH), respectively.

the case for example in phosphate hydrolysis reactions. Thus, we focused here on studying the trend in the directed evolution conversion of phosphotriesterases (pdPTE) to arylesterase (R18).³⁵ Not only that understanding the molecular origin of the change in catalysis can be very instructive but we also have a chance to better understand the issue of functional trade-offs that has been highlighted in some recent works (e.g., refs 35–37). This type of trade-off has been found in studies of metabolic pathways,³⁸ trends in bacterial evolution,³⁹ population sizes,⁴⁰ rates of mutations,⁴¹ and the emergence of antibiotic resistance.⁴² Trade-offs have also been discussed in the context of protein evolution.^{43–46} Nevertheless, the way by which trade-offs affect the evolutionary trajectory remains unclear. In addition, it is not clear that directed evolution follows the same path as natural evolution.²¹ The molecular basis of these phenomena is unclear.

PTE is a bacterial enzyme that accelerates the hydrolysis of organophosphorus pesticides and nerve agents.^{47,48} The active site of PTE (Figure 1A) contains a binuclear zinc center bridged probably by a hydroxide ion and a carboxylated lysine residue.^{49,50} Four histidine residues (His55, His57, His201, and His230), and an aspartate (Asp301), complete the first coordination sphere around the zinc ions. The naturally existing PTE (from *Pseudomonas diminuta* (pdPTE)) catalyzes the hydrolysis of the pesticide paraoxon (Figure 1B) with high efficiency ($k_{\text{cat}}/K_{\text{M}} = 2.2 \times 10^7 \text{ M}^{-1} \text{ s}^{-1}$)³⁵ also possesses a weak, promiscuous, arylesterase activity (catalyzes the hydrolysis of 2-naphthyl hexanoate (2NH; Figure 1C) with $k_{\text{cat}}/K_{\text{M}} = 4.2 \times 10^2 \text{ M}^{-1} \text{ s}^{-1}$).³⁵ Recent directed evolution experiments successfully guided (after 18 rounds of evolution) wild type pdPTE toward exhibiting enhanced arylesterase activity ($k_{\text{cat}}/K_{\text{M}}(2\text{NH}) = 1.7 \times 10^7 \text{ M}^{-1} \text{ s}^{-1}$).³⁵ Although both pdPTE and R18 catalyze hydrolysis reactions, the bond being broken (P–O versus C–O) and the

progression of the reaction (pentavalent intermediate versus tetrahedral intermediate) are radically different.

An interesting issue, that appears to be of major importance in the present case, is the relationship between the Zn–Zn distance and the catalytic effect in the paraxon and the ester systems. Here we have a unique problem that has not been studied carefully in the case of enzyme catalysis. This problem is explored in the present work by a quantum mechanical analysis of the intrinsic dependence of the surface on the Zn–Zn distance as well as the effect of the enzyme on this distance.

Overall, we demonstrate here that combining the EVB approach with DFT electronic structure calculations allows one to explore the effect of different mutations on enzyme catalysis even when we have very complex mechanistic options. Further studies with our approaches should increase the understanding of the role of particular mutations in moving between the two activities.

II. THEORETICAL TREATMENT

In the present case there is a significant controversy about the actual hydrolysis mechanism.^{51–62} For example, some proposals for the paraoxon reaction in pdPTE (or related systems) have favored a start of the nucleophilic attack with an RS that involves a central OH^- ,^{53,58,60,61} whereas refs 51, 54, 57, 62 proposed a TS that involves a proton transfer to Asp301 (mechanism M-2 in Figure 2A), while ref 58 favored a mechanism that is similar to mechanism M-1 of Figure 2A and ref 53 considered a concerted attack of the OH^- ion and a release of leaving group. Reference 55 considered an RS with a central OH^- but then a dissociative TS where the OH^- attack seems to occur after the TS. However, we note that the corresponding surface was not evaluated or calibrated by *ab initio* (DFT) calculations but by semiempirical approach that

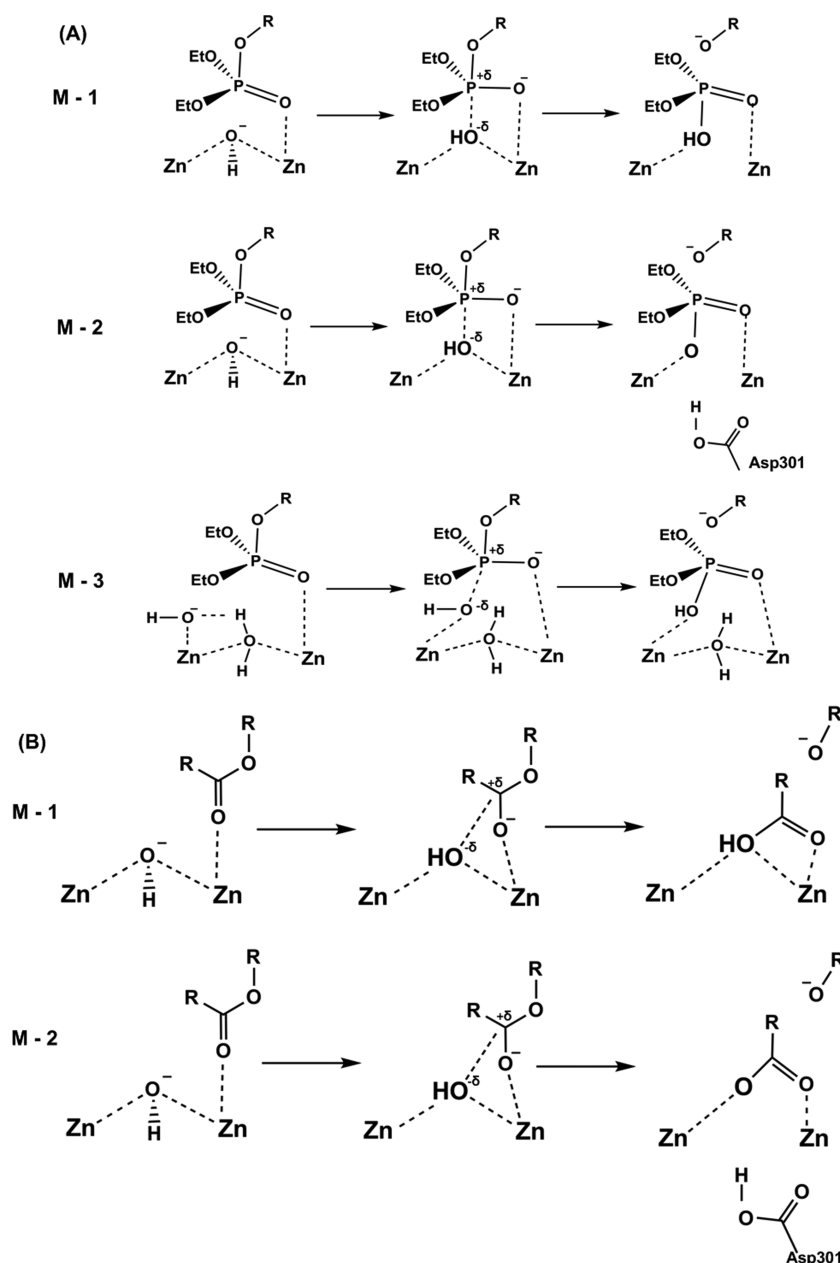


Figure 2. Alternative mechanistic pathways for the hydrolysis of paraoxon (A) and 2-naphthyl hexanoate (2NH) (B). In mechanisms 1 and 2 (M-1 and M-2), the reaction is initiated by a nucleophilic attack of the bridging OH^- on to the substrates in an associative manner, leading to the formation of a pentavalent (A) or tetrahedral (B) (DMNPP and PP, respectively) intermediate (step-1). In step-2, following M-1, the departure of the leaving group (R-O^-) is associated with the formation of a P-OH/C-OH bond, whereas in M-2, the departure of the leaving group (R-O^-) is associated with a simultaneous proton transfer from the nucleophilic OH^- to Asp301, leading to the formation of a P-O/C-O bond. In M-3, the reaction is facilitated by the sideways attack of OH^- ion. However, in this case, the nucleophile is not optimally oriented for inline attack on substrates. Hence when the reaction occurs in the enzyme active site, the protein has to spend an extra amount of energy to create a configuration optimal for catalysis, and thus, this mechanism is not explored in the present work.

might give unreliable TS. Jackson and co-workers⁵⁶ considered an interesting mechanism with a central H_2O and an OH^- which is bound to $\text{Zn}(\alpha)$. This OH^- attacks the phosphate, and the central water transfers its proton to another group (this mechanism has some similarity to mechanism M-3 in Figure 2A). Zhang and co-workers⁵⁹ considered a mechanism where the attacking OH^- is bound to $\text{Zn}(\alpha)$. Overall it is most likely that, at $\text{pH} = 7$, OH^- rather than H_2O is bound between the two Zn ions, and the situation can change with other metal ions (see, e.g., ref 51), although careful para dynamics (PD) calculations of the

relevant pK_a would be very instructive. As much as the esterase activity of the binuclear zinc center is concerned, there are less mechanistic proposals, but one may look for variations of the paraoxon mechanisms.

Considering the above mechanistic uncertainty we have to try to explore the free energy surfaces for several mechanistic options. Here we focused on the mechanistic options described in Figure 2, which appear to be the most likely options. In view of the key role of the two Zn catalytic center we have to use QM cluster calculations in our study of the energetics of the reference reactions (see below and also ref

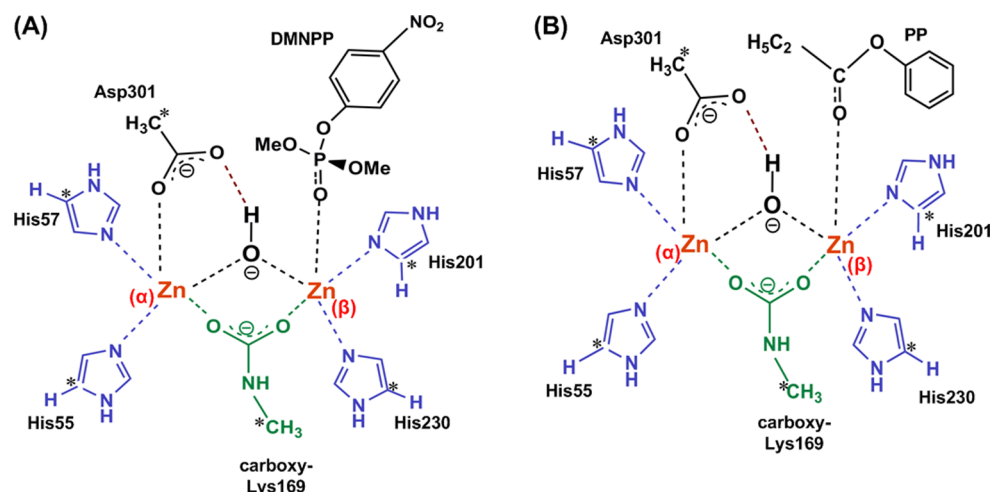


Figure 3. Schematic representation of the active site of pdPTE (the QM cluster) used for modeling the hydrolysis of DMNPP (A) and phenyl propanoate (PP) (B). The Zn atoms and their ligands (His55, His57, His230, His201, Asp301, Lys169, and the bridging nucleophilic OH[−]) are depicted explicitly. The asterisks indicate atoms fixed to their corresponding X-ray positions during the energy minimizations.

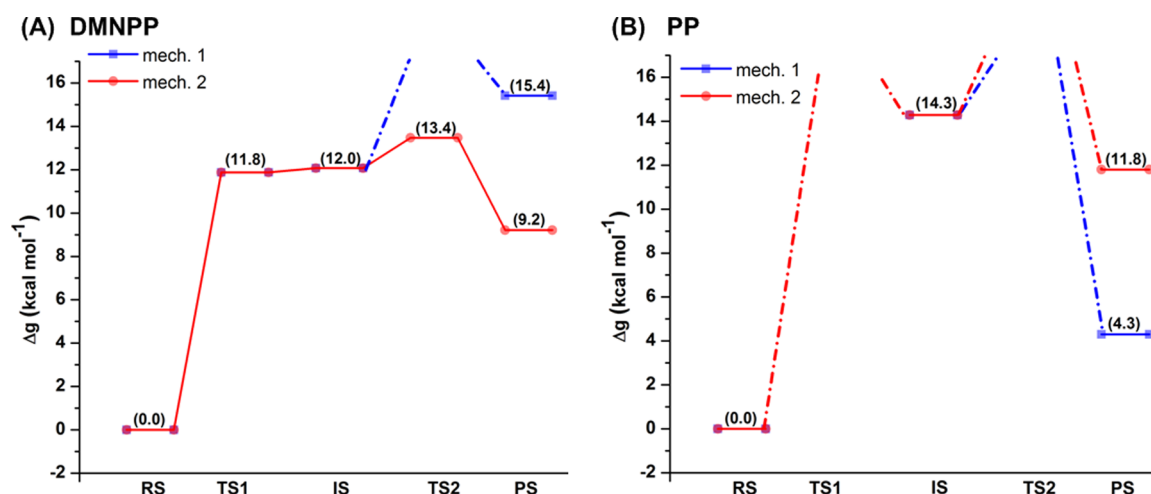


Figure 4. Calculated potential energy profiles for the hydrolysis via mechanisms 1 and 2 (M-1 and M-2 of Figure 2) of dimethyl 4-nitrophenyl phosphate (DMNPP; which serves as a model for paraoxon) (A) and phenyl propanoate (PP; model used for 2NH) (B). The calculations were performed using the QM cluster models (see Figure 3 and Table 1) at a metal–metal (Zn–Zn) distance corresponding to the minimum energy pathway (3.8 Å). The geometries of the critical points (the RS, IS, and PS) along the surfaces were minimized at the B3LYP/6-31+G* level, and the energies of the resulting geometries were computed at the B3LYP/6-311++G(2d,2p) level. The energetics of TS1 and TS2 along the surface of DMNPP (A) (following mechanism 2) were estimated using the results of ref 54 for the corresponding calculated energy differences between these states and the IS. The calculations did not involve optimization of the TSs for paraoxon in the M-1 mechanism and of PP in the M-1 and M-2 mechanisms; these optimizations were considered to be too demanding (and not essential for the present study). The treatment of the barriers in the protein is discussed in the text and in Table 2.

63), but before doing so we started with a qualitative study, evaluating the 2D DFT surfaces for the solution reactions without the Zn ions (see details in the Supporting Information). The corresponding surface for the hydrolysis of triester is given in Supporting Information Figure S1. The surface indicates that the hydrolysis reaction proceeds in an associative manner. However, the energetics of the critical points (RS, IS, PS, and TS's) along the reaction coordinate cannot be deduced from this surface as the quantum model considered for the generation of this surface do not provide an effective reference reaction for the catalysis in the enzyme active site, where the generation of a classical description of the effect of the binuclear Zn cluster is not a simple task (for, e.g., using a dummy atom model etc.). Thus, we focused on DFT calculations with the substrate and the two Zn system in

cluster calculations, where the ligands for the Zn ions are included (see Figure 3). More specifically, the cluster was constructed using the X-ray structure 1HZY and the docked paraoxon or 2NH substrates (the details of the docking protocol are described below). The quantum chemical model includes two zinc ions and the ligands of their first shell, the bridging hydroxide, the carboxylated Lys169, the four histidines (His55, His57, His201, and His230), as well as the catalytic (in mechanism 2) Asp301. The ligands were truncated so that only the side chains were kept. Thus, the histidines were modeled as imidazoles, the aspartate as acetate, and the carboxylated lysine by a carboxylated methylamine. The net charge of the model was +1. The paraoxon substrate was truncated to dimethyl 4-nitrophenyl phosphate (DMNPP), and the 2-naphthyl hexanoate (2NH)

was truncated to phenyl propanoate (PP), which are bound to the more solvent exposed β -Zn site. To retain the strain of the surrounding enzyme on the active site, the atoms that connect the cluster to the protein were kept fixed at their positions in the protein. The constraint on the few fixed points still allowed the other atoms of the cluster to relax.

The cluster model was used to explore the most likely mechanistic options, which are presented in Figure 2. In mechanisms 1 and 2 (M-1 and M-2), the reactions are initiated by a nucleophilic attack of the bridging OH^- on to the substrates in an associative manner, leading to the formation of a pentavalent (Figure 2A) or tetrahedral (Figure 2B) (DMNPP and PP, respectively) intermediate (step-1). In step-2, following M-1, the departure of the leaving group ($\text{R}-\text{O}^-$) is associated with the formation of a $\text{P}-\text{OH}/\text{C}-\text{OH}$ bond, whereas in M-2, the departure of the leaving group ($\text{R}-\text{O}^-$) is associated with a simultaneous proton transfer from the nucleophilic OH^- to Asp301, leading to the formation of a $\text{P}-\text{O}/\text{C}-\text{O}$ bond. In M-2, the reaction is facilitated by a sideways attack of OH^- ion. However, in this case, the nucleophile is not optimally oriented for inline attack on substrates. Hence when the reaction occurs in the protein active site, the protein requires spending an extra amount of energy to create a state optimal for catalysis, and thus, this mechanism is not explored in the present work. At any rate, the results from the cluster calculations for mechanisms 1 and 2 for the hydrolysis of DMNPP and PP are summarized in Figure 4. In assessing the cluster energetics for PP we also considered the estimate from the thermodynamic cycle of Figure S3 of the Supporting Information, which indicates that the barrier for mechanism 2 is significantly higher than that for mechanism 1.

In exploring the mechanistic issues we noted, as stated above, that the Zn–Zn distance can have an impact on the activation barrier. Our study of this issue involved *ab initio* (DFT) examination of the variation of the RS and IS energies on the Zn–Zn distance using quantum cluster models. The corresponding results, which are summarized in Table 1, indicate that the reactant state (RS) in DMNPP involves a slightly larger Zn–Zn distance than that for the PP. The distance effect is larger in the IS. In the case of PP, as will be seen below, the dependence on the Zn–Zn distance can be quite significant in the protein active site.

The above analysis was taken into account in constructing the relevant EVB surfaces. That is, the EVB surfaces were constructed on the basis of the DFT surfaces of the cluster and relevant experimental information. Considering the importance of the Zn ions, we constructed an EVB model with the two Zn ions, their first shell ligands, the nucleophile, and the substrates (see Supporting Information Figure S2). More specifically, in principle we could have tried to take the reference reaction as the solution reaction (where the corresponding activation reactions are $17.5 \text{ kcal mol}^{-1}$ ⁶⁴ and $14.0 \text{ kcal mol}^{-1}$ ⁶⁵ for the DMNPP and PP, respectively) and then add the Zn ions classically. However, it is equally valid (except in exploring the absolute catalytic effect) to take the reaction in the wild-type enzyme as the reference reaction when investigating mutations of the wild type. Thus, we included in the EVB model the Zn ions and calibrated the EVB surfaces by fitting it to the *ab initio* (DFT) cluster results for short (3.3 Å) and long (3.8 Å) Zn–Zn distances in the RS and IS.

Table 1. Dependence of the *ab Initio* (DFT) Energetics, for the Hydrolysis of Dimethyl 4-nitrophenyl Phosphate (DMNPP) and Phenyl Propanoate (PP), on the Zn–Zn Distances at the RS and IS States.^a

Zn–Zn distance in Å	RS	IS
	DMNPP	
3.3	0.0	14.08
3.5	−1.94	$13.59 - 1.94 = 11.65$
3.8	−0.06	$12.13 - 0.06 = 12.07$
	PP	
3.3	0.0	14.67
3.5	−0.5	$12.98 - 0.5 = 12.48$
3.8	2.63	$11.65 + 2.63 = 14.28$

^aAll the energies are in kcal/mol. The table gives the calculated *ab initio* (DFT) energies of the RS (reference) \rightarrow IS (relative to the RS) (see Figure 2) for the hydrolysis of DMNPP and PP using the QM cluster models (see Figure 3) at various Zn–Zn distances. All the geometries are minimized at the B3LYP/6-31+G* level, and the energies of the resulting geometries are computed at the B3LYP/6-311++G(2d,2p) level. The numbers in the RS corresponds to the relative difference in the total *ab initio* (DFT) energy associated with the change in Zn–Zn distances from 3.3 Å \rightarrow 3.5/3.8 Å at the RS ($(\Delta E^{(3.3 \rightarrow 3.5/3.8)})_{\text{RS}}$). The IS energies (relative to the RS) are corrected accordingly.

Here the EVB reference solution models used were very similar to the DFT cluster models with the only exception being that the side chains of the first shell ligands coordinated to the Zn ions (Figure 3 and Figure S2 of the Supporting Information) were not truncated. The atoms indicated by asterisk in Figure 3 were fixed, and their bonds with the rest of the protein were cut. In addition, the nonbonded interactions between the cluster atoms and the protein environment, as well as within the protein environment, were set to zero. The final calibrated parameters are given in Supporting Information Table S1 and the energetics in Table 2 (under EVB reference solution).

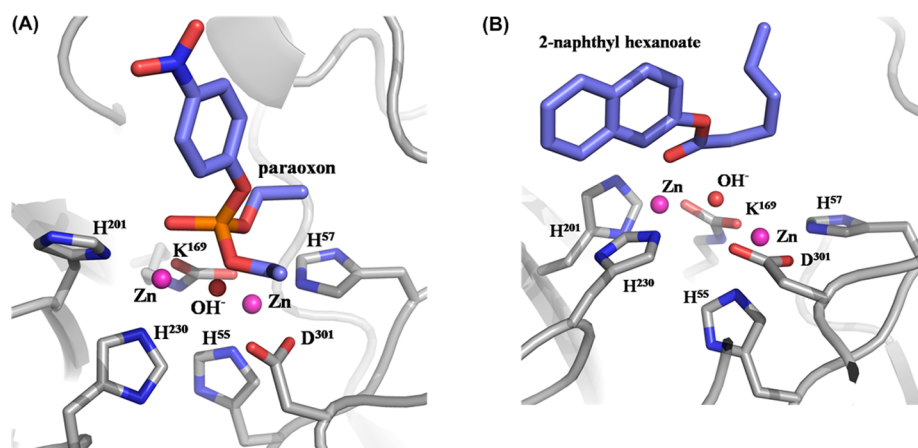
The EVB simulations were performed by the MOLARIS program⁶⁶ using the ENZYMI force field. The activation barriers were calculated by our energy perturbation umbrella sampling (FEP/US) approach (e.g., refs 19, 23). The simulated systems were solvated by the surface constrained all atom solvent (SCAAS) model⁶⁶ with a water sphere of 18 Å radius around the substrates and surrounded by a 2 Å grid of Langevin dipoles and finally by a bulk solvent. The long-range electrostatic effects were treated by our local reaction field (LRF) method.⁶⁶ Systematic validation studies were done within a 22 Å radius of the inner sphere. The EVB calculations started with 200 ps relaxation run followed by 21 frames of 10 ps FEP mapping steps (with time step of 1 fs) using the SCAAS model. The simulations were performed at a temperature of 300 K. The FEP frame simulations were repeated 3–5 times with different initial conditions (obtained from arbitrary points on the relaxation trajectory) in order to obtain reliable results.

The starting coordinates of the pdPTE and R18 were obtained from Protein Data Bank (pdPTE PDB 1HZY;⁴⁹ R18 PDB 4E3T³⁵). The paraoxon and 2-naphthyl hexanoate substrates (Figure 1B and 1C, respectively) were built into the free enzymes using the AutoDock 4.0 software.⁶⁷ The paraoxon ligand was prepositioned within the binding pocket, on the basis of the knowledge from X-ray crystallographic structure similar to the ligand placement in *Agrobacterium*

Table 2. Energetics of the Hydrolysis of Paraoxon and 2-Naphthyl Hexanoate (2NH) in Solution and in the Active Sites of pdPTE and R18 at Various Zn–Zn Distances^a

protein/Zn–Zn distance in Å	$\Delta g_{\text{g}^{\ddagger}(\text{obs})}^{\text{b}}$	QM-cluster ^c		EVB ref solution ^d		$\Delta G_{1\rightarrow 2}^{\circ}$ (protein–calib against cluster) ^f		$\Delta g_{\text{g}^{\ddagger}(2\rightarrow 3)}^{\text{g}}$ (M-1)	$\Delta g_{\text{g}^{\ddagger}(2\rightarrow 3)}^{\text{g}}$ (M-2)	$\Delta g_{\text{g}^{\ddagger}(1\rightarrow 3)}^{\text{g}}$ (M-1) ^g	$\Delta g_{\text{g}^{\ddagger}(1\rightarrow 3)}^{\text{g}}$ (M-2) ^h
		RS	IS	RS ^e	IS ^e	RS	IS				
Paraoxon											
pdPTE	12.9										
3.3		0.0	14.08	0.0	14.08	0.0	14.9	3.3	1.1	18.2	16.0
3.8		−0.06	12.07	−0.25	12.07	2.54	10.2	2.7	2.7	12.9	12.9
R18	17.6										
3.3						0.0	17.9	4.5	11.6	22.4	29.5
3.8						1.28	16.7	3.3	6.9	20.0	23.6
2NH											
pdPTE	19.2										
3.3		0.0	14.67	0.0	14.67	2.6	15.3	2.5	0.0	17.8	15.3 + <i>x</i>
3.8		2.63	14.28	3.13	14.28	0.0	11.16	5.2	8.5	16.4	19.7 + <i>x</i>
R18	13.4										
3.3						7.6	23.6	1.5	3.2	25.1	26.8 + <i>x</i>
3.8						0.0	14.5	0.0	7.9	14.5	22.4 + <i>x</i>

^aAll the energies are in kcal/mol. ^bThe experimentally observed free energy barriers. Note that the observed activation barriers are not always equal to the activation barriers of the chemical step. That is, as discussed in ref 51, in the case of slow substrates k_{cat} is correlated with the chemical step (k_3), while in the case of a fast reaction k_{cat} is correlated with the product release step (k_5). ^cThe QM cluster energies at various Zn–Zn distances as described in Table 1. ^dThe RS (reference) \rightarrow IS (relative to RS) energies obtained using the EVB reference solution models. Here the reference solution models used are very similar to the *ab initio* (DFT) cluster models, with the only exception being that the side chains of the first shell ligands (Figure 3 and Supporting Information Figure S2) that are coordinated to the Zn atoms are not truncated. In addition, the nonbonded interactions between the EVB atoms and the protein environment, as well as within the protein environment, are explicitly set to zero. Also, as in the *ab initio* (DFT) calculations, the atoms represented with asterisk in Figure 3 are fixed during the simulation. The simulations are carried out following exactly the same protocol as that of the protein simulations. The constructed RS \rightarrow IS EVB reference free energy profiles are calibrated against the corresponding *ab initio* (DFT) results presented in Table 1. ^eThe harmonic potentials ($10.0 \cdot (d - 4.2)^2$) (at the RS) and ($27.0 \cdot (d - 4.4)^2$) (at the IS) are explicitly added to the EVB potential while simulating the chemical reactions. Here d is the Zn–Zn distance and the parameters K ($=10.0 \text{ kcal mol}^{-1} \text{ \AA}^{-2}$) and the equilibrium value ($=4.2 \text{ \AA}$) (at the RS) are calibrated in such a way that the computed $(\Delta E^{(3.3 \rightarrow 3.5/3.8)})_{\text{RS}}$ values are close to the corresponding *ab initio* (DFT) values as depicted in Table 1. Similarly the potentials ($10.0 \cdot (d - 4.1)^2$) (at RS) and ($20.0 \cdot (d - 3.3)^2$) (at the IS) were added to the EVB potentials while simulating the 2NH hydrolysis. ^fThe EVB energies for the RS \rightarrow IS movement in the active sites of pdPTE and R18 at the corresponding Zn–Zn distances. The RS energy includes explicitly the value of $(\Delta E^{(3.3 \rightarrow 3.8)})_{\text{RS}}$. ^gThe computed activation free energy barriers for the hydrolysis (via mechanism M-1) of the indicated substrates, at the active sites of pdPTE and R18, at various Zn–Zn distances. ^hThe computed activation free energy barriers (via mechanism M-2) for the hydrolysis of the indicated substrates, at the active sites of pdPTE and R18, at various Zn–Zn distances. The energy of the IS for the hydrolysis of the paraoxon substrate was evaluated by using the EVB model calibrated on the reference reaction of the cluster. The barrier for the second step was adjusted for both mechanisms by forcing (using H_{23}) the lowest calculated barrier to reproduce the observed barrier in pdPTE and then using the same parameters for all the other cases. The barriers for the 2NH reaction in the protein were adjusted so that the lowest calculated barrier in R18 is close to the observed barrier. The parameter x was chosen to reflect our conclusion (see Supporting Information Figure S3) that the barrier for mechanism M-2 is significantly higher than that of mechanism M-1.

**Figure 5.** Spatial orientation of the docked paraoxon (A) and 2-naphthyl hexanoate (2NH) (B) in the active sites of pdPTE and R18 proteins, respectively.

radiobacter (arPTE) protein (phosphotriesterase family, PDB: 2R1N⁶⁸). The 2-naphthyl hexanoate (2NH) ligand was

prepositioned within the binding pocket based on the knowledge from X-ray crystallographic structure similar to

the transition state analog of 2NH (hexylphosphonate 2-naphthyl ester) placement in R18 arylesterase variant of pdPTE³⁵ and archaeon *Sulfolobus solfataricus* (*SsoPox*) protein (lactonase family; PDB: 2VC7⁵⁸). The resulting structures were used as the starting point in docking studies. The automated docking of the ligands to the pdPTE and R18 was performed using the AutoDock's standard protocol (similar to our previous studies⁶⁹). There were 100 independent docking runs with the AutoDock 4.0 program that generated several reasonable ligand conformations. The preferred ligand conformations were determined on the basis of known biological and modeling data, and used in generating the starting structures for the MD simulations. The crystal waters were removed, and all the water molecules were added using the MOLARIS package.⁷⁰ The generated protein complexes (that includes the protein, bound ligand, water, and Langevin dipoles) were pre-equilibrated for 200 ps with a time steps of 1 fs using the ENZYMIK force field,⁶⁶ first with strong constraints at 30 K and then with a gradual heating to 300 K and the simultaneous release of constraints. The residues Lys82, Asp105, Arg225, Asp232, Asp233, Asp253, Arg275, and Arg280 were charged explicitly during the simulations of pdPTE. In the simulations of R18 we also ionized Arg254. In ionizing the above residues we tried several options considering the highly charged metal center, and we adopted a procedure where we assigned 0.5 charge unit instead of a full charge, to compensate for not using the polarizable force field. Lys169, Asp301, and the two Zn ions were part of the EVB region, and their charges, that reflect charge transfer effects, were determined by the *ab initio* (DFT) calculations and are given in Supporting Information Table S1. The structures of the docked paraoxon and 2-naphthyl hexanoate substrates bound to the active sites of pdPTE and R18 proteins are given in Figure 5.

As discussed in our previous works,^{71,72} the experimentally observed behavior can be described by the three state model depicted in Figure 6. More specifically, we can start by using

$$\Delta g^\ddagger = \max(\Delta g_{12}^\ddagger, \Delta g_2^\ddagger) \quad (1)$$

where Δg^\ddagger is the actual overall activation barrier, $\max(x, y)$ is equal to the largest value of the pair of variables x and y , and $\Delta g_2^\ddagger = \Delta g_{23}^\ddagger + \Delta G_{12}$. Although we evaluate the activation

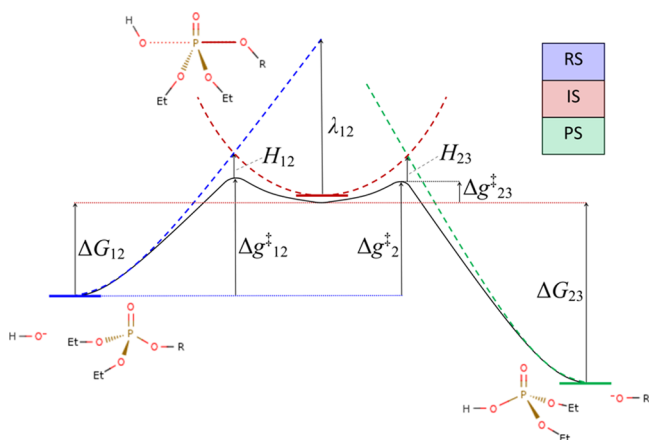


Figure 6. Schematic description of a 3-state EVB model and the corresponding LFER parameters. The specific states depicted are corresponding to the M-1 mechanism.

barriers Δg_{ij}^\ddagger by the full EVB calculations, they can also be estimated by^{23,73}

$$\Delta g_{ij}^\ddagger = \frac{(\Delta G_{ij} + \lambda_{ij})^2}{4\lambda_{ij}} - H_{ij}(x^\ddagger) + \frac{H_{ij}^2(x_r^0)}{\Delta G_{ij} + \lambda_{ij}} \quad (2)$$

where λ_{ij} , ΔG_{ij} , and H_{ij} are the reorganization energy, the reaction energy, and the off diagonal mixing term, respectively. The effect of the specific environment is introduced by controlling the reorganization energies λ_{ij} and/or by changing the value of ΔG_{ij} . In the case where Δg_2^\ddagger is rate-limiting we will see an effect on Δg^\ddagger when there is stabilization of the leaving group, whereas when Δg_{12}^\ddagger is rate-limiting the same stabilization of the leaving group will not affect the rate. Thus we can estimate the activation barrier by considering the LFER between the log of the rate constant, k , and the pK_a of the leaving group (which can be related to ΔG_{23}). That is, the LFER can be written as

$$\Delta \log k = \beta \Delta pK_{lg} \quad (3)$$

where β is a scalar constant. This can be expressed in terms of the corresponding free energy differences as

$$\Delta \Delta g^\ddagger / 2.3RT = -\beta \Delta \Delta G_{23} / 2.3RT \quad (4)$$

where Δg^\ddagger is the rate-limiting barrier. Now we can consider the two cases above by writing:

Case 1 (for $\Delta g_{12}^\ddagger < \Delta g_2^\ddagger$):

$$\begin{aligned} \beta &= -\Delta \Delta g_2^\ddagger / \Delta \Delta G_{23} = -\Delta \Delta G_{12} / \Delta \Delta G_{23} \\ &- (\Delta G_{23} + \Delta g_{23}^\ddagger)^2 / 4\lambda_{23} \Delta \Delta G_{23} \simeq -\frac{(\Delta G_{23} + \lambda_{23})}{2\lambda_{23}} \end{aligned}$$

Case 2 (for $\Delta g_{12}^\ddagger > \Delta g_2^\ddagger$):

$$\beta = -\Delta \Delta g_2^\ddagger / RT \Delta \Delta G_{23} = 0 \quad (5)$$

This equation can guide us in assessing the effect of the stabilization of the leaving group. Note, however, when the pK_a of the leaving group changes, the resulting change in ΔG_{12} may not be reflected by eq 5 (which is for ΔG_{23} rather than the pK_a).

III. RESULTS AND DISCUSSION

In order to progress in understanding the evolutionary trend in moving from paraoxonase to arylesterase it is important to have the ability to reproduce the observed catalytic effects of different design constructs as well as those of natural active sites. Thus, we assess here our ability to reproduce the trend in the observed catalytic effect. In trying to accomplish this task we started by considering the possible dependence of the catalytic effect on the Zn–Zn distance. In doing so we noted that the observed distances in pdPTE and R18 are 3.3 and 3.8 Å, respectively, whereas a new carefully structural study (Jackson's personal communications) of the mutant R22 (that catalyzes 2NH), and a revertant (R0) (that catalyzes the hydrolysis of paraoxon), found that the observed distances in R0 and R22 are 3.7 and 3.3 Å, respectively. Considering the difficulty in determining the metal–metal distances in proteins we added to our calculation strategy the requirement to evaluate the free energy of changing the Zn–Zn distance in each protein and with each substrate. To explore this issue we started by evaluating the free energy difference for moving

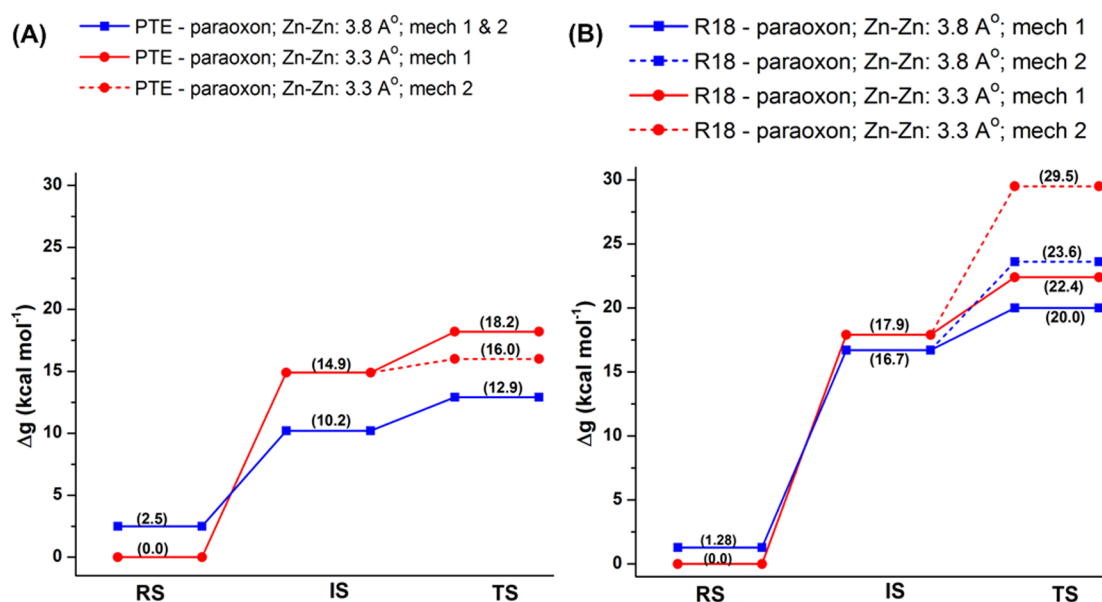


Figure 7. EVB free energy profiles for the hydrolysis of paraoxon by pdPTE (A) and R18 (B) via mechanisms 1 and 2 (M-1 and M-2 of Figure 2) at Zn–Zn distances of 3.3 and 3.8 Å. The RS energy for a Zn–Zn distance of 3.3 Å is used as the reference, and the relative free energy difference associated with the change in Zn–Zn distance from 3.3 Å → 3.8 Å at the RS is explicitly included in the profiles.

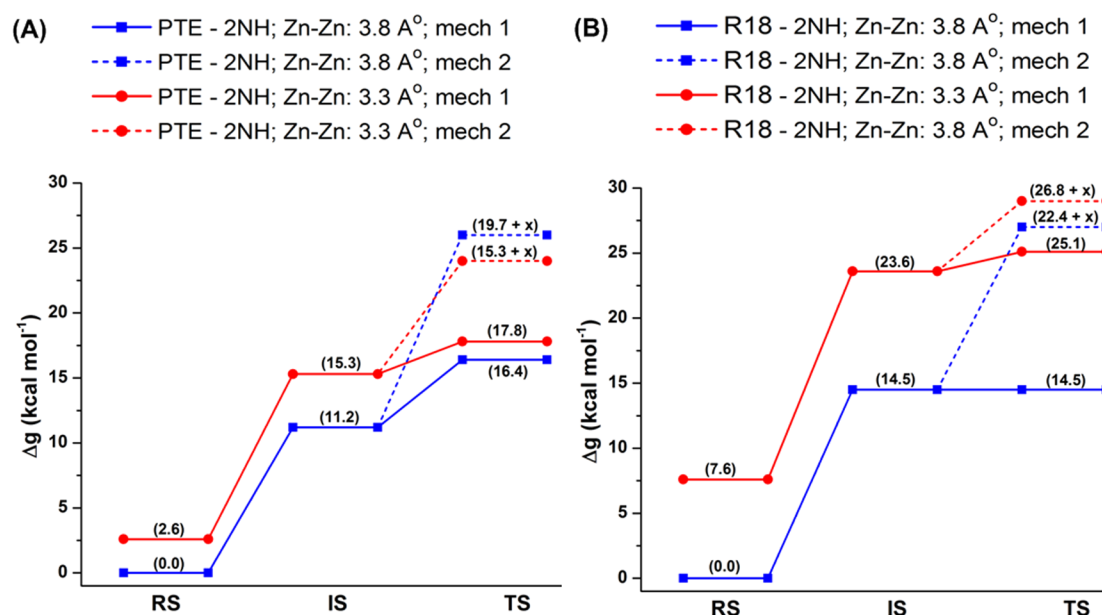


Figure 8. EVB free energy profiles for the hydrolysis of 2-naphthyl hexanoate (2NH) by pdPTE (A) and R18 (B) via mechanisms 1 and 2 (M-1 and M-2 of Figure 2) at Zn–Zn distances of 3.3 and 3.8 Å. The RS energy for a Zn–Zn distance of 3.8 Å is used as the reference, and the relative free energy difference associated with the change in Zn–Zn distance from 3.8 Å → 3.3 Å at the RS is explicitly included in the profiles. Meaning of parameter x is described in the notes of Table 2.

between the initial and final values of the Zn–Zn distance using FEP calculations. This was done for the Zn–Zn distance in pdPTE and R18 for the RS of both paraoxon and 2NH. The dependence on this distance in the IS was then obtained by fixing it (in 3.3 and 3.8 Å) when performing the EVB calculations described below. The corresponding calculated effects of the change of the Zn–Zn distance are incorporated in the results reported in Table 2.

While considering the Zn–Zn distance dependence we started with systematic EVB simulations of the paraoxon hydrolysis in the pdPTE and R18 enzymes. Our study considered mechanisms M-1 and M-2 of Figure 2. The

corresponding results of the EVB simulations are summarized in Table 2 and Figure 7. Similarly we explored the trend for the 2NH ester, which is summarized in Table 2 and Figure 8. In constructing Table 2, we tried to use the observed barriers in the enzyme in the calibration process. That is, since we are dealing primarily with mutation effects and not with the absolute catalysis we could force the lowest calculated barrier to be similar in each mechanism to be similar to the observed barrier. This allowed us to overcome the need for evaluating the activation barrier in the reference cluster reaction which would require careful and demanding calculations. More specifically, the barrier for the second step was adjusted for

both mechanisms by forcing (using H_{23}) the lowest calculated barrier to reproduce the observed barrier in pdPTE and then using the same parameters for all the other cases. The barriers for the 2NH reaction in the protein were adjusted so that the lowest calculated barrier in R18 is closed to the observed barrier. The barrier for mechanism M-2 was determined using a parameter x , that reflected our conclusion (see Supporting Information Figure S3) that the barrier for mechanism M-2 is significantly higher than that of mechanism M-1.

In both the paraoxon and the 2NH cases we reproduced the observed trend. That is, looking at the paraoxon results we see that in pdPTE we have similar barriers for mechanism 1 and 2. Now, the two mechanisms still have similar barriers in R18, but the barriers increase significantly. In the case of 2NH (Figure 8) we see that mechanism 1 has the lowest barrier in both pdPTE and R18, but the barrier is significantly lower in R18. Now, if we take the lowest barrier in each case we find that the observed compensating trend is reproduced, where the barrier of the paraoxon increases upon moving from pdPTE to R18, and the barrier of 2NH decreases.

Interestingly, the lowest energies of the RS in the paraoxon case are obtained at 3.3 Å Zn–Zn distances for both pdPTE and R18 (although in R18 the energies at 3.3 and 3.8 Å are close). On the other hand, for 2NH the lowest energies in the RS are for a distance of 3.8 Å, but with larger tendency to be at the 3.8 Å distance in R18. However, in both cases the least energy distance at the TS is at 3.8 Å. Note that (regardless of the actual least energy distance) the tendency to be at 3.8 Å separation increases upon moving from pdPTE to R18.

The nature of the second barrier is of interest in terms of its relationship to the observed LFER³⁵ (Supporting Information Figure S4). That is, the LFER of the phosphate triesters seems to indicate that in pdPTE the rate-determining step is the first step while in the case of R18 the second barrier is rate-limiting. This trend can be rationalized considering the similarity of the height of the TS and the first intermediate in pdPTE. Here, a modest barrier for the first step will rationalize the observed results. In the case of 2NH we have an interesting finding where the second barrier is not rate-limiting (Figure 8) in R18. This seems to rationalize the observed LFER³⁵ in R18, where we do not have a dependence on the leaving group. However, in pdPTE the calculations produce a rate-limiting second barrier, which is inconsistent with the corresponding experimental LFER where the absence of slope seems to exclude a rate-limiting second barrier. Nevertheless, it is still possible that the first barrier (TS1 in Figure 4) is higher than the IS and is the actual rate-limiting barrier.

It is also useful to point out that while the large reduction in paraoxon catalysis upon moving to R18 is easily reproduced, the corresponding increase in catalysis of 2NH is not fully reproduced here. However, since the increase in barrier for paraoxon is overestimated perhaps the fact that the barrier for 2NH is not increasing upon moving to R18 is encouraging. It is also interesting that, despite the significant dependence on the Zn–Zn distance, it does not seem to affect the change in activity upon moving from pdPTE to R18 (comparing the change in barrier moving from 3.3 to 3.8 Å). Here looking at other systems such as R22 and R0 would be informative.

IV. CONCLUDING REMARKS

Designing enzymes with large catalytic power is a challenge that is unlikely to be met without the ability to predict the stabilization and the corresponding TSs. Estimating the catalytic effect by applying gas phase models or even by evaluating the electrostatic interaction between the TS and different residues is not expected to reproduce the observed rate acceleration since it is impossible to estimate the preorganization effect without including the protein and evaluating the activation free energy or at least its linear response approximation (LRA) estimate.

It seems to us that a proper screening strategy should be able to reproduce the observed catalytic power and to predict the effect of different mutations. Semiempirical MO-QM/MM studies can in principle be useful in exploring this major requirement, but the predicted trend in the protein (e.g., ref 74) is not yet satisfactory. Here one of the problems is not having sufficiently reliable potential surfaces (which appear to be a major challenge for bi nuclear zinc enzymes). Here one can try to use QM(ai)/MM calculations, but then the problem is the requirement for very extensive sampling. In principle one may try to use QM(ai)/MM with the paradynamics (PD) approach,⁷⁵ but this approach would still require a major sampling on the classical reference potential and will require enormous computer time. In this respect the quantitative results obtained by the current and previous EVB studies are clearly encouraging.

The present work highlights a major challenge in computational enzyme design, namely capturing the effect of the configuration of the metal ions catalytic center. That is, although we have studied extensively systems with two metal ions such as DNA polymerases,^{76–80} the distance between the two metal ions has not been a major catalytic issue. Here on the other hand, the two metal ions act as one catalytic center with the central OH^- , and thus, the control of the metal–metal distance is crucial and is an integral part of the catalytic machinery. In fact, the situation might be similar in other systems such as β lactamases (see ref 81). Here the current study only provides an initial glimpse on the possibility that design consideration may have to consider the control of the Zn–Zn distance and further studies, including exploration of the effect of the metal–metal distance in other variants (e.g., R22 and R0) where the observed trend in the distance may reflect a different situation than in pdPTE and R18.

At this point we would like to reclarify that we have demonstrated the ability to reproduce quantitatively the absolute catalytic effects and mutational effects in naturally evolved enzymes¹⁹ and in designer enzymes (this work and our previous studies^{20,21,33}). This indicates that the catalytic effect of enzymes, that must be considered in enzyme design, is not associated with elusive effects (e.g., conformational dynamics⁸²), but with electrostatic preorganization.^{19,83} In fact, not only has the problem with the implications that catalysis is associated with dynamical effects been clarified and demonstrated (e.g., refs 84, 85), but also very recent work (refs 86, 87) actually demonstrated experimentally the fact that dynamics is not helpful in designs. Although it is still not widely clear that in cases of significant barrier in large molecules passing barriers do not reflect dynamical effect but the corresponding Boltzmann chance for random fluctuations (ref 84). In fact, no consistent simulation study has ever reproduced a significant observed catalytic effect by dynamical

effects, and the same is likely to remain true for design efforts. Of course, there is an unjustified tendency to argue that some proposed catalytic effects have not been modeled in naturally evolved enzymes and in designer enzymes. In this respect it is useful to note that modeling features such as conformational exploration, substrate floppiness, pK_a values of key residues, and the effect of water molecules (that were mentioned for example in some reviews of computational enzyme design (e.g., ref 88)) have been an integral part of our modeling at least since 1986 (e.g., see refs 16, 18, 23, 25, 89). On the other hand, it seems to us that some of the key and most visible enzyme design studies involved gas phase (or related) modeling that cannot reproduce the observed catalysis in known enzyme substrate complexes. It seems rather clear that systematic computer aided enzyme design must involve approaches such as the EVB that can actually reproduce the observed catalytic effect.

As discussed above, the mechanism of the hydrolysis of paraoxon and 2NH is not fully clear. Thus, simulating the catalysis in several feasible mechanistic options is quite important. It is also important to use electronic structure DFT calculations with cluster models in the calibration process. Doing so indicates that mechanism M-1 is the most likely mechanism for both the paraoxon and ester.

Although we and others have very encouraging experience with the use of the EVB in enzyme modeling, the present two-Zn systems present a new element of complexity where the calibration of the EVB requires the use of an *ab initio* (DFT) cluster model. In this respect it is likely that use of the EVB as reference potential in PD calculations to consistently sample *ab initio* (DFT) surfaces in the enzyme may be an effective strategy despite its cost. This is clearly true with regards to gaining more confidence in the current results.

It should also be noted here that the incorporation of the two Zn ions in the EVB region allowed us to avoid the need of a getting special treatment for the ions (e.g., the dummy atoms treatment of refs 90, 91). That is, a realistic first sphere geometry around the Zn ions is easily obtained when the ions and their surrounding ligands are included in the EVB subsystem and calibrated by cluster calculations.

Overall we consider the present work partially as an exploratory search of the role of metal–metal distance in the directed evolution of the catalysis of paraoxon and 2NH. Here our main finding is that the issue is complex and should be taken into account in design studies rather than a unique conclusion on the importance of this factor.

■ ASSOCIATED CONTENT

■ Supporting Information

Details about the generation of the solution free energy surfaces corresponding to the hydrolysis of triester without Zn ions, EVB parameters used, the active sites of pdPTE complexed with paraoxon and 2NH, the thermodynamic cycle used to determine the energetics associated with the states corresponding to the IS \rightarrow PS pathway for the hydrolysis of PP, and the observed LFER for the hydrolysis of paraoxon and 2NH. This material is available free of charge via the Internet at <http://pubs.acs.org>.

■ AUTHOR INFORMATION

Corresponding Author

*E-mail: warshel@usc.edu.

Author Contributions

^{||}(R.P.B., M.J.L.M., M.P.F.) These authors contributed equally.

Notes

The authors declare no competing financial interest.

■ ACKNOWLEDGMENTS

This work was supported by NIH Grant GM24492. We gratefully thank Professors Colin J. Jackson, Nobuhiko Tokuriki, and Dan S. Tawfik for stimulating discussion and for sharing results with us before publication. M.P.F. thanks the Cancer Research Institute Irvington Fellowship for financial support. We thank the University of Southern California's High Performance Computing and Communication Center (HPCC) for computer time.

■ REFERENCES

- (1) Toscano, M. D.; Woycechowsky, K. J.; Hilvert, D. Minimalist Active-Site Redesign: Teaching Old Enzymes New Tricks. *Angew. Chem., Int. Ed.* **2007**, *46*, 3212–3236.
- (2) Hilvert, D. Design of Protein Catalysts. *Annu. Rev. Biochem.* **2013**, *82*, 447–470.
- (3) Kiss, G.; Çelebi-Ölçüm, N.; Moretti, R.; Baker, D.; Houk, K. N. Computational Enzyme Design. *Angew. Chem., Int. Ed.* **2013**, *52*, 5700–5725.
- (4) Korendovych, I. V.; DeGrado, W. F. Catalytic Efficiency of Designed Catalytic Proteins. *Curr. Opin. Struct. Biol.* **2014**, *27*, 113–121.
- (5) Arnold, F. H.; Volkov, A. A. Directed Evolution of Biocatalysts. *Curr. Opin. Chem. Biol.* **1999**, *3*, 54–59.
- (6) Khersonsky, O.; Rothlisberger, D.; Dym, O.; Albeck, S.; Jackson, C. J.; Baker, D.; Tawfik, D. S. Evolutionary Optimization of Computationally Designed Enzymes: Kemp Eliminases of the KE07 Series. *J. Mol. Biol.* **2010**, *396*, 1025–42.
- (7) Zhao, H.; Chockalingam, K.; Chen, Z. Directed Evolution of Enzymes and Pathways for Industrial Biocatalysis. *Curr. Opin. Biotechnol.* **2002**, *13*, 104–110.
- (8) Goldsmith, M.; Tawfik, D. S. Directed Enzyme Evolution: Beyond the Low-Hanging Fruit. *Curr. Opin. Struct. Biol.* **2012**, *22*, 406–412.
- (9) Gould, S. M.; Tawfik, D. S. Directed Evolution of the Promiscuous Esterase Activity of Carbonic Anhydrase II. *Biochemistry* **2005**, *44*, 5444–5452.
- (10) Tracewell, C. A.; Arnold, F. H. Directed Enzyme Evolution: Climbing Fitness Peaks One Amino Acid at a Time. *Curr. Opin. Chem. Biol.* **2009**, *13*, 3–9.
- (11) Reetz, M. T. Biocatalysis in Organic Chemistry and Biotechnology: Past, Present, and Future. *J. Am. Chem. Soc.* **2013**, *135*, 12480–12496.
- (12) Wijma, H. J.; Janssen, D. B. Computational Design Gains Momentum in Enzyme Catalysis Engineering. *FEBS J.* **2013**, *280*, 2948–2960.
- (13) Baker, D. An Exciting but Challenging Road Ahead for Computational Enzyme Design. *Protein Sci.* **2010**, *19*, 1817–1819.
- (14) Li, X.; Zhang, Z.; Song, J. Computational Enzyme Design Approaches with Significant Biological Outcomes: Progress and Challenges. *Comput. Struct. Biotechnol. J.* **2012**, *2*, e201209007.
- (15) Pantazes, R. J.; Grisewood, M. J.; Maranas, C. D. Recent Advances in Computational Protein Design. *Curr. Opin. Struct. Biol.* **2011**, *21*, 467–472.
- (16) Frushicheva, M. P.; Mills, M. J. L.; Schopf, P.; Singh, M. K.; Prasad, R. B.; Warshel, A. Computer Aided Enzyme Design and Catalytic Concepts. *Curr. Opin. Chem. Biol.* **2014**, *21*, 56–62.
- (17) Fuxreiter, M.; Mones, L. The Role of Rreorganization Energy in Rational Enzyme Design. *Curr. Opin. Chem. Biol.* **2014**, *21*, 34–41.

- (18) Roca, M.; Vardi-Kilshtain, A.; Warshel, A. Toward Accurate Screening in Computer-Aided Enzyme Design. *Biochemistry* **2009**, *48*, 3046–3056.
- (19) Warshel, A.; Sharma, P. K.; Kato, M.; Xiang, Y.; Liu, H.; Olsson, M. H. M. Electrostatic Basis for Enzyme Catalysis. *Chem. Rev.* **2006**, *106*, 3210–3235.
- (20) Frushicheva, M. P.; Cao, J.; Warshel, A. Challenges and Advances in Validating Enzyme Design Proposals: The Case of Kemp Eliminase Catalysis. *Biochemistry* **2011**, *50*, 3849–3858.
- (21) Frushicheva, M. P.; Cao, J.; Chu, Z. T.; Warshel, A. Exploring Challenges in Rational Enzyme Design by Simulating the Catalysis in Artificial Kemp Eliminase. *Proc. Natl. Acad. Sci. U.S.A.* **2010**, *107*, 16869–74.
- (22) Labas, A.; Szabo, E.; Mones, L.; Fuxreiter, M. Optimization of Reorganization Energy Drives Evolution of the Designed Kemp Eliminase KE07. *Biochim. Biophys. Acta* **2013**, *1834*, 908–917.
- (23) Warshel, A. *Computer Modeling of Chemical Reactions in Enzymes and Solutions*; John Wiley & Sons: New York, 1991.
- (24) Warshel, A.; Sussman, F. Toward Computer-Aided Site-Directed Mutagenesis of Enzymes. *Proc. Natl. Acad. Sci. U.S.A.* **1986**, *83*, 3806.
- (25) Hwang, J. K.; Warshel, A. Semiquantitative Calculations of Catalytic Free Energies in Genetically Modified Enzymes. *Biochemistry* **1987**, *26*, 2669–2673.
- (26) Liu, H.; Warshel, A. The Catalytic Effect of Dihydrofolate Reductase and Its Mutants is Determined by Reorganization Energies. *Biochemistry* **2007**, *46*, 6011–6025.
- (27) Ram Prasad, B.; Plotnikov, N. V.; Lameira, J.; Warshel, A. Quantitative Exploration of the Molecular Origin of the Activation of GTPase. *Proc. Natl. Acad. Sci. U.S.A.* **2013**, *110*, 20509–20514.
- (28) Marti, S.; Andres, J.; Moliner, V.; Silla, E.; Tunon, I.; Bertran, J. Computer-Aided Rational Design of Catalytic Antibodies: The 1F7 Case. *Angew. Chem., Int. Ed.* **2007**, *46*, 286–290.
- (29) Marti, S.; Andres, J.; Moliner, V.; Silla, E.; Tunon, I.; Bertran, J. Predicting an Improvement of Secondary Catalytic Activity of Promiscuous Isochorismate Pyruvate Lyase by Computational Design. *J. Am. Chem. Soc.* **2008**, *130*, 2894–2895.
- (30) Mulholland, A. J. Computational Enzymology: Modelling the Mechanisms of Biological Catalysts. *Biochem. Soc. Trans.* **2008**, *36*, 22–26.
- (31) Chudyk, E. I.; Limb, M. A. L.; Jones, C.; Spencer, J.; van der Kamp, M. W.; Mulholland, A. J. QM/MM Simulations as an Assay for Carbapenemase Activity in Class A β -Lactamases. *Chem. Commun.* **2014**, *50*, 14736–14739.
- (32) van der Kamp, M. W.; Mulholland, A. J. Combined Quantum Mechanics/Molecular Mechanics (QM/MM) Methods in Computational Enzymology. *Biochemistry* **2013**, *52*, 2708–2728.
- (33) Roca, M.; Vardi-Kilshtain, A.; Warshel, A. Toward Accurate Screening in Computer-Aided Enzyme Design. *Biochemistry* **2009**, *48*, 3046–3056.
- (34) Frushicheva, M. P.; Cao, J.; Warshel, A. Challenges and Advances in Validating Enzyme Design Proposals: The Case of Kemp Eliminase Catalysis. *Biochemistry* **2011**, *50*, 3849–3858.
- (35) Tokuriki, N.; Jackson, C. J.; Afriat-Jurnou, L.; Wyganowski, K. T.; Tang, R. M.; Tawfik, D. S. Diminishing Returns and Tradeoffs Constrain the Laboratory Optimization of an Enzyme. *Nat. Commun.* **2012**, *3*, 1257.
- (36) Tawfik, D. S. Accuracy-Rate Tradeoffs: How Do Enzymes Meet Demands of Selectivity and Catalytic Efficiency? *Curr. Opin. Chem. Biol.* **2014**, *21*, 73–80.
- (37) Kaltenbach, M.; Tokuriki, N. Dynamics and Constraints of Enzyme Evolution. *J. Exp. Zool., Part B* **2014**, *322*, 468–487.
- (38) Chou, H. H.; Chiu, H. C.; Delaney, N. F.; Segre, D.; Marx, C. J. Diminishing Returns Epistasis Among Beneficial Mutations Decelerates Adaptation. *Science* **2011**, *332*, 1190–1192.
- (39) Khan, A. I.; Dinh, D. M.; Schneider, D.; Lenski, R. E.; Cooper, T. F. Negative Epistasis Between Beneficial Mutations in an Evolving Bacterial Population. *Science* **2011**, *332*, 1193–1196.
- (40) Miralles, R.; Moya, A.; Elena, S. F. Diminishing Returns of Population Size in the Rate of RNA Virus Adaptation. *J. Virol.* **2000**, *74*, 3566–3571.
- (41) Arjan, J. A.; Visser, M.; Zeyl, C. W.; Gerrish, P. J.; Blanchard, J. L.; Lenski, R. E. Diminishing Returns From Mutation Supply Rate in Asexual Populations. *Science* **1999**, *283*, 404–6.
- (42) MacLean, R. C.; Perron, G. G.; Gardner, A. Diminishing Returns From Beneficial Mutations and Pervasive Epistasis Shape the Fitness Landscape for Rifampicin Resistance in *Pseudomonas Aeruginosa*. *Genetics* **2010**, *186*, 1345–1354.
- (43) Aharoni, A.; Gaidukov, L.; Khersonsky, O.; Gould, S. M.; Roodveldt, C.; Tawfik, D. S. The ‘Evolvability’ of Promiscuous Protein Functions. *Nat. Genet.* **2005**, *37*, 73–76.
- (44) Khersonsky, O.; Roodveldt, C.; Tawfik, D. S. Enzyme Promiscuity: Evolutionary and Mechanistic Aspects. *Curr. Opin. Chem. Biol.* **2006**, *10*, 498–508.
- (45) Poelwijk, F. J.; de Vos, M. G.; Tans, S. J. Tradeoffs and Optimality in the Evolution of Gene Regulation. *Cell* **2011**, *146*, 462–70.
- (46) Amar, D.; Berger, I.; Amara, N.; Tafa, G.; Meijler, M. M.; Aharoni, A. The Transition of Human Estrogen Sulfotransferase from Generalist to Specialist Using Directed Enzyme Evolution. *J. Mol. Biol.* **2012**, *416*, 21–32.
- (47) Dumas, D. P.; Caldwell, S. R.; Wild, J. R.; Raushel, F. M. Purification and Properties of the Phosphotriesterase from *Pseudomonas diminuta*. *J. Biol. Chem.* **1989**, *264*, 19659–65.
- (48) Donarski, W. J.; Dumas, D. P.; Heitmeyer, D. P.; Lewis, V. E.; Raushel, F. M. Structure-Activity Relationships in the Hydrolysis of Substrates by the Phosphotriesterase from *Pseudomonas diminuta*. *Biochemistry* **1989**, *28*, 4650–4655.
- (49) Benning, M. M.; Shim, H.; Raushel, F. M.; Holden, H. M. High Resolution X-ray Structures of Different Metal-Substituted Forms of Phosphotriesterase from *Pseudomonas Diminuta*. *Biochemistry* **2001**, *40*, 2712–2722.
- (50) Vanhooke, J. L.; Benning, M. M.; Raushel, F. M.; Holden, H. M. Three-Dimensional Structure of the Zinc-Containing Phosphotriesterase with the Bound Substrate Analog Diethyl 4-Methylbenzylphosphonate. *Biochemistry* **1996**, *35*, 6020–6025.
- (51) Aubert, S. D.; Li, Y.; Raushel, F. M. Mechanism for the Hydrolysis of Organophosphates by the Bacterial Phosphotriesterase. *Biochemistry* **2004**, *43*, 5707–5715.
- (52) Jackson, C.; Kim, H.-K.; Carr, P. D.; Liu, J.-W.; Ollis, D. L. The Structure of an Enzyme–Product Complex Reveals the Critical Role of a Terminal Hydroxide Nucleophile in the Bacterial Phosphotriesterase Mechanism. *Biochim. Biophys. Acta* **2005**, *1752*, 56–64.
- (53) Grimsley, J. K.; Calamini, B.; Wild, J. R.; Mesecar, A. D. Structural and Mutational Studies of Organophosphorus Hydrolase Reveal a Cryptic and Functional Allosteric-Binding Site. *Arch. Biochem. Biophys.* **2005**, *442*, 169–179.
- (54) Chen, S. L.; Fang, W. H.; Himo, F. Theoretical Study of the Phosphotriesterase Reaction Mechanism. *J. Phys. Chem. B* **2007**, *111*, 1253–1255.
- (55) Wong, K.-Y.; Gao, J. The Reaction Mechanism of Paraoxon Hydrolysis by Phosphotriesterase from Combined QM/MM Simulations. *Biochemistry* **2007**, *46*, 13352–13369.
- (56) Jackson, C. J.; Foo, J.-L.; Kim, H.-K.; Carr, P. D.; Liu, J.-W.; Salem, G.; Ollis, D. L. In Crystallo Capture of a Michaelis Complex and Product-Binding Modes of a Bacterial Phosphotriesterase. *J. Mol. Biol.* **2008**, *375*, 1189–1196.
- (57) Kim, J.; Tsai, P.-C.; Chen, S.-L.; Himo, F.; Almo, S. C.; Raushel, F. M. Structure of Diethyl Phosphate Bound to the Binuclear Metal Center of Phosphotriesterase. *Biochemistry* **2008**, *47*, 9497–9504.
- (58) Elias, M.; Dupuy, J.; Merone, L.; Mandrich, L.; Porzio, E.; Moniot, S.; Rochu, D.; Lecomte, C.; Rossi, M.; Masson, P.; Manco, G.; Chabriere, E. Structural Basis for Natural Lactonase and Promiscuous Phosphotriesterase Activities. *J. Mol. Biol.* **2008**, *379*, 1017–1028.

- (59) Zhang, X.; Wu, R.; Song, L.; Lin, Y.; Lin, M.; Cao, Z.; Wu, W.; Mo, Y. Molecular Dynamics Simulations of the Detoxification of Paraoxon Catalyzed by Phosphotriesterase. *J. Comput. Chem.* **2009**, *30*, 2388–2401.
- (60) Ely, F.; Hadler, K. S.; Gahan, L. R.; Guddat, L. W.; Ollis, D. L.; Schenk, G. The Organophosphate-Degrading Enzyme from *Agrobacterium Radiobacter* Displays Mechanistic Flexibility for Catalysis. *Biochem. J.* **2010**, *432*, 565–573.
- (61) López-Canut, V.; Ruiz-Pernía, J. J.; Castillo, R.; Moliner, V.; Tuñón, I. Hydrolysis of Phosphotriesters: A Theoretical Analysis of the Enzymatic and Solution Mechanisms. *Chem.—Eur. J.* **2012**, *18*, 9612–9621.
- (62) Bigley, A. N.; Raushel, F. M. Catalytic Mechanisms for Phosphotriesterases. *Biochim. Biophys. Acta* **2013**, *1834*, 443–453.
- (63) Liao, R. Z. *Quantum Chemical Cluster Modeling of Enzymatic Reactions*. Ph.D. Dissertation, Stockholm University, Stockholm, Sweden, 2010.
- (64) Fukuto, T. R.; Metcalf, R. L. Reactivity of Some 2-p-Nitrophenoxy-1,3,2-dioxaphospholane 2-Oxides and -Dioxaphosphorinane 2-Oxides. *J. Med. Chem.* **1965**, *8*, 759–762.
- (65) Bruice, T. C.; Mayahi, M. F. The Influence of the Leaving Tendency of the Phenoxy Group on the Ammonolysis and Hydrolysis of Substituted Phenyl Acetates. *J. Am. Chem. Soc.* **1960**, *82*, 3067–3071.
- (66) Lee, F. S.; Chu, Z. T.; Warshel, A. Microscopic and Semimicroscopic Calculations of Electrostatic Energies in Proteins by the POLARIS and ENZYMIK Programs. *J. Comput. Chem.* **1993**, *14*, 161–185.
- (67) Morris, G. M.; Goodsell, D. S.; Halliday, R. S.; Huey, R.; Hart, W. E.; Belew, R. K.; Olson, A. J. Automated Docking Using a Lamarckian Genetic Algorithm and an Empirical Binding Free Energy Function. *J. Comput. Chem.* **1998**, *19*, 1639–1662.
- (68) Jackson, C. J.; Foo, J.-L.; Tokuriki, N.; Afriat, L.; Carr, P. D.; Kim, H.-K.; Schenk, G.; Tawfik, D. S.; Ollis, D. L. Conformational Sampling, Catalysis, and Evolution of the Bacterial Phosphotriesterase. *Proc. Natl. Acad. Sci. U.S.A.* **2009**, *106*, 21631–21636.
- (69) Singh, N.; Warshel, A. Absolute Binding Free Energy Calculations: On the Accuracy of Computational Scoring of Protein–Ligand Interactions. *Proteins: Struct., Funct., Bioinf.* **2010**, *78*, 1705–1723.
- (70) Chu, Z. T.; Villa, J.; Strajbl, M.; Schutz, C. N.; Shurki, A.; Warshel, A. MOLARIS, Version 9.13; University of Southern California: Los Angeles, CA, 2013.
- (71) Aqvist, J.; Kolmodin, K.; Florian, J.; Warshel, A. Mechanistic Alternatives Phosphate Monoester Hydrolysis: What Conclusions can be Drawn from Available Experimental Data? *Chem. Biol.* **1999**, *6*, R71–R80.
- (72) Warshel, A.; Schweins, T.; Fothergill, M. Linear Free Energy Relationships in Enzymes. Theoretical Analysis of the Reaction of Tyrosyl-tRNA Synthetase. *J. Am. Chem. Soc.* **1994**, *116*, 8437–8442.
- (73) Hwang, J. K.; King, G.; Creighton, S.; Warshel, A. Simulation of Free Energy Relationships and Dynamics of SN2 Reactions in Aqueous Solution. *J. Am. Chem. Soc.* **1988**, *110*, 5297–5311.
- (74) Alexandrova, A. N.; Rothlisberger, D.; Baker, D.; Jorgensen, W. L. Catalytic Mechanism and Performance of Computationally Designed Enzymes for Kemp Elimination. *J. Am. Chem. Soc.* **2008**, *130*, 15907–15915.
- (75) Plotnikov, N. V.; Warshel, A. Exploring, Refining, and Validating the Paradynamics QM/MM Sampling. *J. Phys. Chem. B* **2012**, *116*, 10342–10356.
- (76) Fothergill, M.; Goodman, M. F.; Petruska, J.; Warshel, A. Structure-Energy Analysis of the Role of Metal Ions in Phosphodiester Bond Hydrolysis by DNA Polymerase I. *J. Am. Chem. Soc.* **1995**, *117*, 11619–11627.
- (77) Florián, J.; Goodman, M. F.; Warshel, A. Computer Simulation of the Chemical Catalysis of DNA Polymerases: Discriminating Between Alternative Nucleotide Insertion Mechanisms for T7 DNA Polymerase. *J. Am. Chem. Soc.* **2003**, *125*, 8163–8177.
- (78) Prasad, B. R.; Warshel, A. Prechemistry Versus Preorganization in DNA Replication Fidelity. *Proteins* **2011**, *79*, 2900–2919.
- (79) Xiang, Y.; Goodman, M. F.; Beard, W. A.; Wilson, S. H.; Warshel, A. Exploring the Role of Large Conformational Changes in the Fidelity of DNA Polymerase β . *Proteins: Struct., Funct., Genet.* **2008**, *70*, 231–247.
- (80) Xiang, Y.; Oelschlaeger, P.; Florian, J.; Goodman, M. F.; Warshel, A. Simulating the Effect of DNA Polymerase Mutations on Transition State Energetics and Fidelity: Evaluating Amino Acid Group Contribution and Allosteric Coupling for Ionized Residues in Human Pol β . *Biochemistry* **2006**, *45*, 7036–7048.
- (81) Tomatis, P. E.; Fabiane, S. M.; Simona, F.; Carloni, P.; Sutton, B. J.; Vila, A. J. Adaptive Protein Evolution Grants Organismal Fitness by Improving Catalysis and Flexibility. *Proc. Natl. Acad. Sci. U.S.A.* **2008**, *105*, 20605–20610.
- (82) Klinman, J. P.; Kohen, A. Hydrogen Tunneling Links Protein Dynamics to Enzyme Catalysis. *Annu. Rev. Biochem.* **2013**, *82*, 471–496.
- (83) Warshel, A. Energetics of Enzyme Catalysis. *Proc. Natl. Acad. Sci. U.S.A.* **1978**, *75*, 5250–5254.
- (84) Kamerlin, S. C.; Warshel, A. At the Dawn of the 21st Century: Is Dynamics the Missing Link for Understanding Enzyme Catalysis? *Proteins* **2010**, *78*, 1339–75.
- (85) Adamczyk, A. J.; Cao, J.; Kamerlin, S. C. L.; Warshel, A. The Catalytic Power of Dihydrofolate Reductase and Other Enzymes Arises from Electrostatic Preorganization, not Conformational Motions. *Proc. Natl. Acad. Sci. U.S.A.* **2011**, *108*, 14115–14120.
- (86) Tokuriki, N.; Jackson, C. J. Enzyme Dynamics and Engineering: One Step at a Time. *Chem. Biol.* **2014**, *21*, 1259–1260.
- (87) Gobeil, S. M. C.; Clouthier, C. M.; Park, J.; Gagné, D.; Berghuis, A. M.; Doucet, N.; Pelletier, J. N. Maintenance of Native-like Protein Dynamics May Not Be Required for Engineering Functional Proteins. *Chem. Biol.* **2014**, *21*, 1330–1340.
- (88) Khersonsky, O.; Kiss, G.; Röthlisberger, D.; Dym, O.; Albeck, S.; Houk, K. N.; Baker, D.; Tawfik, D. S. Bridging the Gaps in Design Methodologies by Evolutionary Optimization of the Stability and Proficiency of Designed Kemp Elimination KE59. *Proc. Natl. Acad. Sci. U.S.A.* **2012**, *109*, 10358–10363.
- (89) Vardi-Kilshtai, A.; Roca, M.; Warshel, A. The Empirical Valence Bond as an Effective Strategy for Computer-Aided Enzyme Design. *Biotech. J.* **2009**, *4*, 495–500.
- (90) Aqvist, J.; Warshel, A. Free Energy Relationships in Metalloenzyme-Catalyzed Reactions. Calculations of the Effects of Metal Ion Substitutions in Staphylococcal Nuclease. *J. Am. Chem. Soc.* **1990**, *112*, 2860–2868.
- (91) Oelschlaeger, P.; Klahn, M.; Beard, W. A.; Wilson, S. H.; Warshel, A. Magnesium-Cationic Dummy Atom Molecules Enhance Representation of DNA Polymerase beta in Molecular Dynamics Simulations: Improved Accuracy in Studies of Structural Features and Mutational Effects. *J. Mol. Biol.* **2007**, *366*, 687–701.